



Numerical simulation of 3D angle-interlock woven fabric forming and compression processes

Yongqiang Liu¹ · Zhongxiang Pan^{1,2,3} · Jiajia Yu⁴ · Xiaoyu Hong¹ · Zhiping Ying² · Zhenyu Wu^{2,3}

Received: 15 October 2023 / Accepted: 11 March 2024 / Published online: 27 March 2024
© The Author(s), under exclusive licence to Springer-Verlag France SAS, part of Springer Nature 2024

Abstract

This paper provides a modeling method for predicting the internal structure of three-dimensional (3D) angle-interlock woven fabric. Inspired by the digital element method, the numerical model of micro-scale was established by using truss element. The numerical model was compared with the Computed Tomography (CT) cross-sectional scan of the actual fabric sample, and the results were consistent. The mechanical properties of the 3D angle-interlock woven fabric is closely related to the fabric's structure. Therefore, by changing the tension at both ends of the yarn tows to explore the influence on the yarn tows' geometry, it was found that different tensions affects the cross-sectional areas and crimp angles of the yarn tows. On the basis of fabric forming, multi-shape molds were designed to press the fabric into different shapes, which were semi-hexagonal, arc-shaped and L-shaped. The results of numerical simulation showed that the fabric will undergo inter-layer slip when compressed, especially in the region where the mold deformation is large.

Keywords 3D angle-interlock woven fabric · Truss element chains · Yarn tension · Multi-shape molds

Introduction

Fiber reinforced composites have many advantages, such as high specific strength, high specific modulus, fatigue resistance, and designability, and are widely used in construction, shipbuilding, and automotive fields [1–3]. The most significant disadvantage of traditional laminated structural composites is easy delamination and poor impact resistance.

3D textile composites incorporate yarns in the thickness direction, which can well solve the problem of easy delamination of laminated structures. So 3D textile composites have become the main reinforcement structure for fiber-reinforced composite material candidates [4]. 3D textile composites include 3D woven composites, 3D knitted composites, 3D braided composites et al. Among them, 3D woven composites are widely used because of their stable woven process, high degree of automation, relatively low cost, easy molding, and other advantages [5]. 3D woven reinforcement is an essential branch of 3D textiles. The weft yarn is arranged parallel and straight, and the warp yarn intersects the weft layer to layer along the thickness direction of the fabric. In this way, the structure of 3D woven fabrics will be more stable [6, 7]. The geometric shape of the fabric will affect its mechanical properties. Therefore, it is essential to study the influence of different yarn tensions

✉ Zhongxiang Pan
panzx@zstu.edu.cn

✉ Zhiping Ying
zstuyingzp@163.com

Yongqiang Liu
liuyongqiangjiayou@163.com

Jiajia Yu
janice_jiajiayu@163.com

Xiaoyu Hong
ahsxxhy@163.com

Zhenyu Wu
zistwuzhenyu@163.com

¹ College of Textile Science and Engineering, Zhejiang Sci-Tech University, Hangzhou 310018, China

² Faculty of Mechanical Engineering and Automation, Zhejiang Sci-Tech University, Hangzhou 310018, China

³ Zhejiang Provincial Innovation Center of Advanced Textile Technology, Shaoxing 312000, China

⁴ College of Energy Engineering, Zhejiang University, Hangzhou 310027, China

on the geometric shape of the fabric. However, the influence of 3D woven fabrics structure on their mechanical properties mainly depends on experimental tests [8, 9]. Compared with experimental tests, numerical simulation overcomes the constraints of weaving conditions, resulting in greater savings in material and labor as well as rapid prediction of fabric geometry.

As we all know, fabrics are composed of thousands of fibers. Hence, numerical models must be considered at the macro-scale, meso-scale, and micro-scale. The fabric is regarded as a continuous uniform material at the macro-scale with special constitutive properties [10]. Meso-scale refers to the analysis at the yarn level, which is often modeled as a curve with an ideal cross-section [11]. Fibers can be modeled as 'mechanical rods' at the micro-scale to simulate the interaction between fibers [12, 13]. The deformation of yarns in actual fabrics depends on the arrangement and the interactions between fibers. The relative motion of the fibers within the yarn will be manifested as yarn deformation at the macroscopic scale [14].

Up to now, researchers have proposed several micro-scale models to simulate the interactions between fibers to reflect the fabric's actual geometry [15–18]. Wang and Sun [19] first proposed the 'digital unit chain' method, which is a fabric forming process modeling method based on fiber dynamics. In this dynamic model, the yarn is discretized into digital nodal elements with a certain cross section. Hinge links are used between node units. This method provides a variety of complex weaving processes of fabric forming process. Zhou [20] proposed the multi-chain digital element method. In this model, each yarn is modeled as a set of fibers, and each fiber is modeled as a digital chain. Yarn tension and cross-section are determined by fiber tension and arrangement, respectively. The increase in the number of digital chains leads to an increase in the amount of contact calculation, which greatly reduces the efficiency of the micro-level model. In order to solve the efficiency problem, Miao [14] improved the calculation formula of the contact unit and proposed a static relaxation algorithm based on the kinematics of the textile process to establish the micro-geometric of the fabric, which reduced the simulation time significantly. After trying, 19~61 fibers can be more suitable for expressing the path changes and cross-sectional shape changes of the yarn between and within the layers. Dobrich [21, 22] considered the yarn parameters in the weaving process, such as warp density, weft density, yarn size, yarn crimp, and yarn size. Digital element approach (DEA) obtains the microscopic geometry of the fabric, and the simulation results are in good agreement with the actual woven fabric. Mahadik and Hallett [23] proposed a 3D braided structure model with a layer-to-layer angle interlocking structure. A chain of beam elements is modeled for each fiber, and the load is applied to the fabric to simulate the compaction state of the fabric at the

micro-scale. Based on Mahadik and Hallett, Green et al. [24] further used beam elements to model 3D braided structures. Daelemans [25] carried out a numerical model based on truss elements with zero bending stiffness. A circular section truss element represents the fiber in the fabric, and the fabric model is compacted to make it consistent with the actual thickness of the fabric. In the process of fabric compaction, the general contact of Abaqus is used to deal with the interaction between fibers. Sockalingam et al. [26–28] modeled the tow at the fiber level, simulated the deformation of the tow under transverse load, and found that the interaction between the fibers had an essential influence on the geometry of the tow. Therefore, it is necessary to study further the influence of the traction yarn's tension on the fabric's geometric shape. 3D angle-interlock fabrics also have specific applications in aviation, such as aero-engine fan blades [29]. Brittle fracture is unacceptable in this crucial component, and 3D angle-interlock woven can effectively solve this problem. Xiao et al. [30] based on the inextensibility of continuous carbon yarn, the geometrical models for yarn sliding were expressed and verified in order to describe the yarn sliding. Jiao et al. [31] studied the hemispherical forming of 3D layer-to-layer (LTL) preform, analyzed the influence of structural parameters on the forming process, and found that the macroscopic deformation and microstructure change of 3D LTL preform was closely related to the yarn woven structure. Abteu et al. [32] studied the influence of warp and weft density on the in-plane characteristics of 3D interwoven hemispherical molded interlocking preforms.

At present, most of the research focuses on the simulation of fabrics at macro and meso scales. In comparison to the former two, there are few micro-scale studies. In the compression molding of fabrics, the majority of studies are concentrated on hemispherical shapes, with fewer investigations into other shapes. The internal deformation of the formed fabric can be predicted by numerical simulation. It greatly reduces the cost of research. Based on the previous research, this paper proposes a simulation method based on the concept of virtual fiber and digital components to simulate the forming of 3D angle-interlock woven fabric. The truss element chains are carried out to simulate the fibers in the yarn, and the explicit quasi-static finite element framework in Abaqus is used to deal with the deformation of the fabric from the loose state to the mutual contact and fiber-to-fiber contact. The numerical model was compared with the CT scan of the real fabric in two directions along the path of the warp and weft tows. The influence of tension on the cross-sectional shape of the fabric and the yarn path was investigated by changing the tension at both ends of the yarn. In addition, this paper further studied the influence of shaped mold compression on the micro-geometric structure of the fabric. Based on the numerical simulation of fabric forming, compression numerical simulation models were

established to predict the change in the internal structure of the fabric, and the inter-layer shear angle was introduced to quantify the inter-layer deformation of the fabric.

Materials and methods

Weaving process of 3D angle-interlock woven fabric

The 3D angle-interlock woven fabric tightly connects the multi-layer fabric through the binder yarn in the thickness direction of the fabric to form a whole structure. The fabric structure in the research is based on the warp yarn as the binder yarn, which interweaves the adjacent two-layer weft yarn. The material of fabric is glass fiber, which is composed of five-layer warp and six / four-layer weft. It was woven by a 3D self-built loom. There are four main mechanisms: sending mechanism, opening mechanism, weft mechanism, and curl mechanism, as shown in Fig. 1a, b. The warp is in the x-direction, the weft is in the y-direction, and the fabric thickness is in the z-direction. The warp yarns along the z-direction are interlocked with

the weft yarns arranged in parallel along the y-direction, which greatly improves the resistance to delamination ability of the fabric. The weaving principle of the 3D angle-interlock woven fabric is provided in Fig. 1c, d. First, the warp yarn passes through the heald eye on the harness frame along the x-direction. It is divided into five groups. Warp yarn move up and down with the harness frame to form a suitable opening region. The five-layer warp divides the opening region into six clear shed openings along the x-direction, and then the rapier weft insertion mechanism pulls the weft into these six shed openings at the same time. After that, the rapier weft insertion mechanism withdraws from the shed opening, and one weft insertion action is completed. Then, under the traction of the harness frame, two adjacent groups of warp yarns in the y-direction reversely move along the z-direction so that the warp and weft layer are interwoven together. At the same time, the reed pushes the weft yarn to the weaving region. The four-layer weft tow repeats the previous action to complete a weaving cycle.

In this paper, the 3D woven panel preform parameters used are listed in Table 1. The effective size of the whole

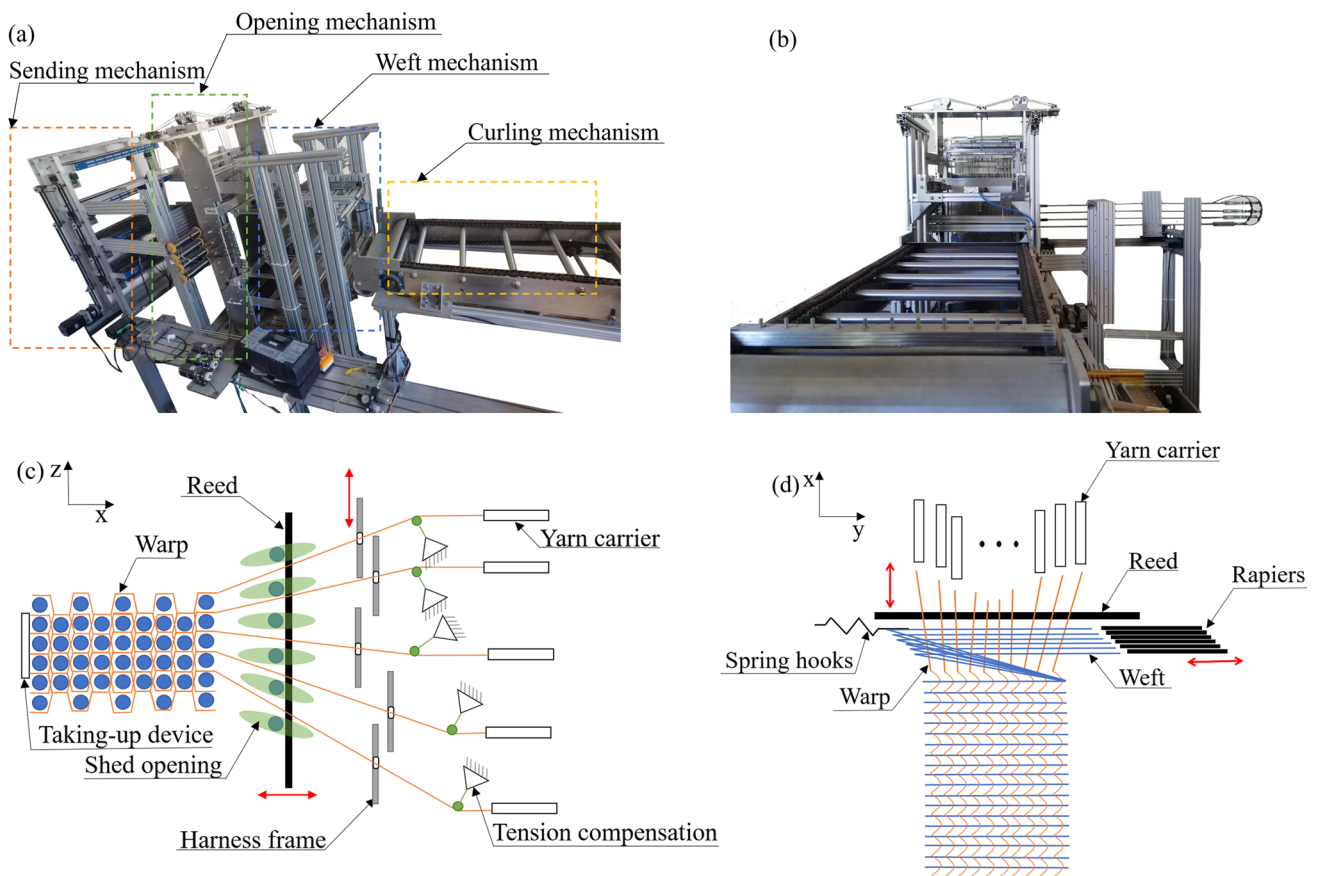


Fig. 1 a, b Self-built weaving machine for fabric preparation; c Lateral view of the weaving process of 3D angle-interlock fabric; d Top view of the weaving process of 3D angle-interlock fabric

Table 1 Architectural parameters of 3D angle-interlock woven fabric

Tows	Yarns specification	Layers	Weave density (ends/cm)
Warp	340tex × 1	5	6.09
Weft	680tex × 1	6/4	4.05

fabric is 426 mm (length) × 344 mm (width) × 3 mm (thickness).

Specimen preparation

The 3D woven composite material studied consists of glass fiber reinforcement and epoxy resin matrix. The 3D angle-interlock woven fabric was obtained by the 3D loom built by the laboratory, as provided in Fig. 2a. After preparing the fabric preform, the epoxy resin (EPOLAM 2040) and its curing agent (EPOLAM 2042) (both provided by AXSON, France) were mixed in a ratio of 100:32 and then infused into the fabric reinforcement by vacuum assisted resin transfer molding (VARTM). The 3D woven fabric is a planar structure, and the curing process of the fabric is shown in Fig. 2b, c. The infiltrated composite was placed at 20 °C for 24 h and then in an oven at 70 °C for 12 h. After cooling, a wire-cutting machine cut the cured fabric into a 10 mm

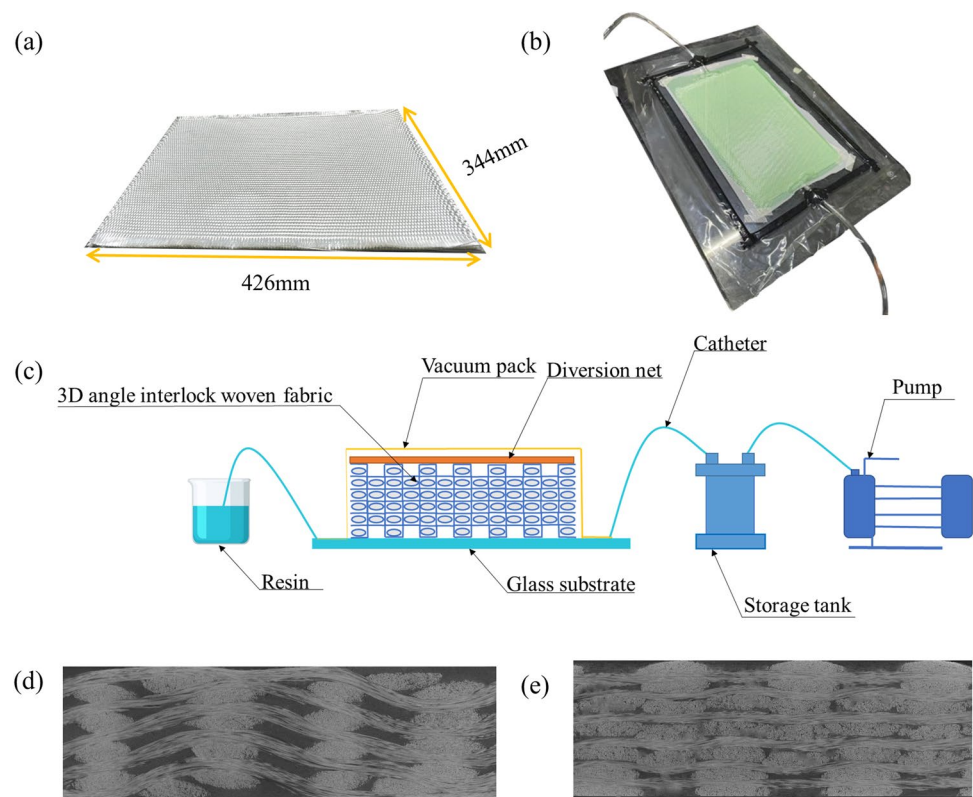
× 10 mm wide sample. The sample was sent to Shanghai Endi Detection and Control Technology Company, which used the Dionod2 high-resolution all-purpose nanofocus CT detection system to take the cross-section of the sample, and the obtained optical image is presented in Fig. 2d, e. The internal structure of the sample (cross-section shape and path of warp and weft tows) can be clearly observed by the cross-section CT scan images. The results show that the fabric reinforcement is well infiltrated and has no obvious bubble.

Modeling methodology

Simplification of the fabric forming process

The fabric forming process is a dynamic process of interaction between yarns. The primary process includes the rapier weft insertion pulling the weft yarn into the shed openings simultaneously. A group of warp yarns is interweaved with weft yarns along the positive direction of the z-axis under the traction of the harness frame, and another set of warp and weft yarns are interweaved layer to layer along the negative direction of the z-axis. Finally, a weaving cycle is completed. In the weaving process, there is contact between the rigid parts of the 3D loom and the flexible yarn, contact between the flexible yarns, and contact between the fibers

Fig. 2 a 3D angle-interlock woven fabric; b, c VARTM process; d, e CT cross-sectional view of the composite



inside the yarn. The weaving process has large deformations and large displacements of the loom's rigid components and yarns. These factors bring great difficulties to numerical simulation. Therefore, we need to simplify the weaving process in the numerical simulation of fabric forming.

After the above description, we mainly model the interweaving between the yarns. Compared with the formed fabric, the initial fabric is in a loose state due to no load applied at both ends. In this section, a numerical simulation is performed for the yarn from a loose state to a load applied at both ends to make it closer to the actual fabric state. From the macro- perspective, it is a whole fabric. From the meso- perspective, it is the interweaving of yarns, and from the micro- perspective, it is the interweaving of yarns consisted of thousands of fibers. Obviously, the increase in the number of virtual fibers in each yarn will better capture the characteristics of the yarn and better simulate the overall mechanical behavior of the yarn. Nevertheless, this will significantly increase the computational cost. Therefore, for a given simulation, we need to select a sufficient number of virtual fibers to achieve the required complexity while providing results within a reasonable time frame. Zhou et al. [20] have done many simulations related to virtual fibers and concluded that 19 to 50 virtual fibers are sufficient to represent the cross-sectional geometry of the yarn. In the numerical model established, the warp tow is composed of 25 virtual fibers, and the weft tow consists of 48 virtual fibers.

Modeling steps

In this part, the overall overview of the 3D angle-interlock woven fabric modeling studied is shown in Fig. 3a-c. The finite element analysis software Abaqus was used to simulate the fabric forming. The process of modeling and simulation

process can be divided into three steps. (1) The Python script written in Abaqus was run to realize the automatic generation of the trajectory shape, mesh, interaction between fibers, load, and analysis step time of the fabric, and got an unsolved fabric model. (The initial fabric obtained by running the python script written by Abaqus was in a zero stress state.) (2) In order to obtain the realistic fabric structure, the Abaqus dynamic explicit solver was used to solve the model, and the initially loose fabric began to stretch under the preset load. (3) To verify the feasibility of the simulation, the numerical simulation results were compared with the fabric's CT scan to verify the numerical simulation's feasibility.

Yarn cross-sectional shape and material properties

Many investigators explored the distribution of virtual fibers in the initial state. The typical arrangement methods were concentric circles and rectangles around the center line. Miao et al. [14] numerically modeled circular and rectangular cross-sections in multi-chain digital element analysis. Each yarn consisted of 19 digital chains. It was found that the shape of the initial beam cross-section had no significant effect on the final geometry. It was concluded that various initial yarn cross-sectional geometries could be used in numerical simulation. This paper used the rectangular cross-section as the initial shape of the yarn cross-section, as shown in Fig. 3a. Both the truss element and beam element could be devoted to simulate virtual fiber. In order to obtain virtual fiber with real material properties and low bending stiffness, virtual fiber based on beam element simulation had large bending stiffness and torsion stiffness, which was not suitable for this model. Since the bending stiffness (K_b) and torsional stiffness (K_t) of the fiber are proportional to the modulus of elasticity (E_f) and rigidity (G_f) and the fourth

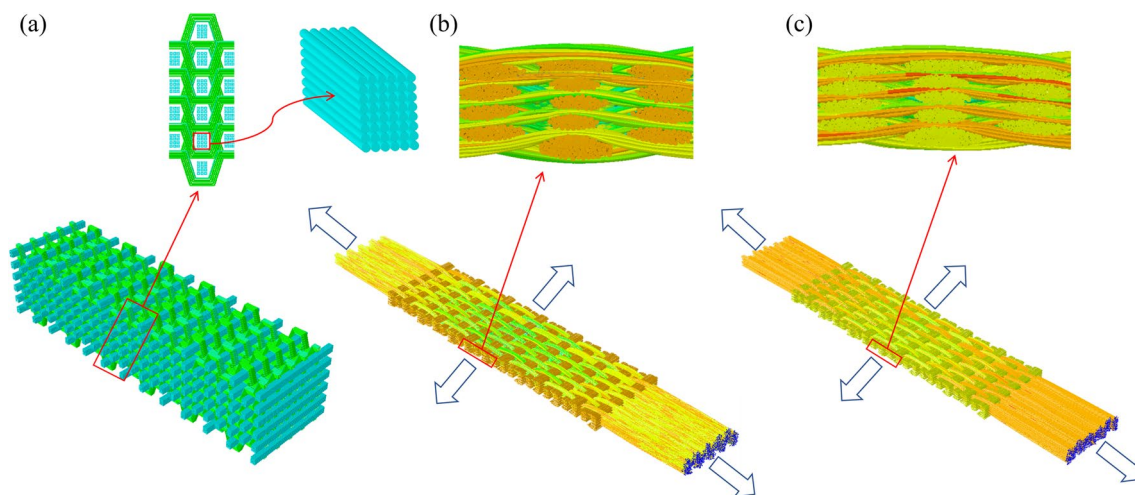


Fig. 3 General overview of the modeling workflow: **a** A Python script generated the initial Woven fabric geometry in Abaqus FEA software; **b** The state after applying a load at the end of the initial fabric; **c** The end of fabric simulation forming

power of fiber diameter (D_f). The details were shown in Eqs. (1) and (2). Considering the calculation cost, the yarn will be discretized into fewer virtual fibers, so the diameter of the virtual fiber is much larger than the actual fiber, so the virtual fiber has larger bending stiffness and torsional stiffness. So as to solve this problem, the previous researchers would use the elastic-plastic material model or artificially reduce the bending stiffness [33]. The truss element was used to simulate the virtual fiber because the bending stiffness of the virtual fiber based on the element was basically zero, so there was no need to reduce the bending stiffness artificially, and the fiber could use the actual elastic modulus. In addition, the truss element was the simplest finite element, consisting of two nodes. Each node had three degrees of freedom, which would make the virtual fiber simulation based on the truss element more efficient. Each fiber was constructed using a T3D2 truss unit chain.

$$K_b = \left(\pi E_f D_f^4 \right) / 64 \quad (1)$$

$$K_t = \left(\pi G_f D_f^4 \right) / 32 \quad (2)$$

Contact detection

This paper used the general contact algorithm of Abaqus/Explicit to detect the contact between virtual fibers. General contact allows the automatic detection of multiple regions. The tangential behavior between virtual fibers selected the penalty friction formula. Because there will be large displacement and large deformation when the virtual fiber begins to stretch from both ends of the relaxation state, to minimize the penetration between the virtual fibers, the hard contact was selected in the normal behavior of the virtual fibers.

Loading strategy and fabric forming boundary conditions

The load forces of 3 N and 2.5 N were added steadily at both ends of the warp and weft, respectively. The magnitude of the load force is proportional to the model size and the friction coefficient between the fibers. If the load is applied immediately at both ends of the yarn, it may cause the stress wave to shake during the propagation of the truss unit chain, which will cause fiber blockage during the stretching process. This unfavorable effect was removed by ramping up the loading smoothly from zero to the maximum value. In this section, the fabric was in a loose state at the beginning of the numerical simulation. There was no interweaving between the warp and weft yarns. At the fabric boundary, a concentrated force load was applied from both ends of the warp and weft yarns to simulate the loading force condition before and

after the interweaving of the warp and weft yarns and the interweaving process, as shown in Fig. 4. During the loading process, the fibers were rearranged to form a realistic yarn cross-section. The weft tension remains unchanged before and after weaving and during the process. The warp tension will gradually increase with the harness frame's upper and lower. The analysis step time reaches the set value, which also represents the end of fabric forming. At this time, the two ends of the fiber of the whole model are straight. There is no irregular winding of the fibers in the interweaving region of warp and weft. They show that the fabric is well formed.

In order to facilitate the change of the size of the model, further exploration is needed. The initial weft is in a straight state, and the parameters can be changed. The initial warp is undulating, so the warp is adopted to use a periodic unit as shown in the red mark in Fig. 5a. The adjacent warp yarns in the y-axis direction are symmetrical about the x-axis direction, as shown in Fig. 5a, b. In order to ensure that the load at the boundary of the warp cycle unit can be transmitted, it is necessary to set the offset distance to ensure that the ends of the warp cycle unit coincide in the x-axis direction.

Virtual fiber contact

In forming 3D angle interlock woven fabric, the yarns will contact and squeeze each other. The fabric is characterized by contact and extrusion between fibers at the micro-scale. The contact will occur when the distance between the center lines of the two virtual fibers is less than the diameter of the virtual fiber. When the contact occurs, the physical phenomena are divided into two types. Adhesion, that is, the two units adhere to each other and remain relatively static; The two units slip each other, and relative motion occurs. These two physical phenomena can be represented by the friction relationship as follows.

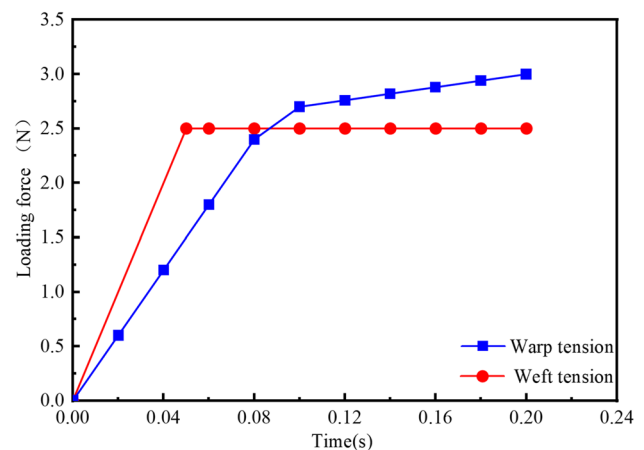


Fig. 4 The link between step time and yarn tension

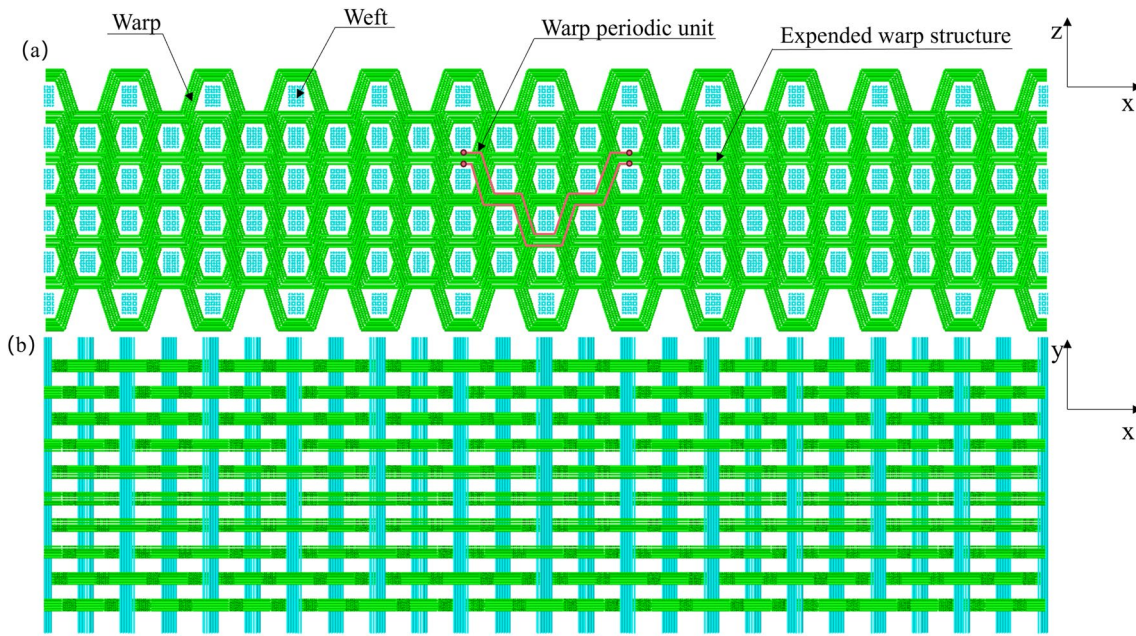


Fig. 5 Warp periodic units and extended warp structure: a Lateral view of the model; b Top view of the model

$$f^{equ} < f^{crit} \tag{3}$$

$$f^{equ} \geq f^{crit} \tag{4}$$

where f^{equ} is the equivalent frictional force and f^{crit} is the critical force; these two tangential forces can be expressed as

$$f^{equ} = \sqrt{f_1^2 + f_2^2} \tag{5}$$

$$f^{crit} = \mu \cdot p \tag{6}$$

where f_1 and f_2 denote the tangential component of the contact surface, μ is the friction coefficient, and p is the normal force of the contact surface. The normal force can be written as a function of the overclosure, h .

$$p = p(h) \tag{7}$$

$$h = \| X_f - Y_f \| - (R_x + R_y) \tag{8}$$

where h denotes the penetration distance after the unit contact, and the normal force is a function of the unit penetration distance. X_f and Y_f are the center points of the unit of the fiber, R_x and R_y are the radius of the element. The normal force of the unit is proportional to the penetration distance of the unit. The unit penetration distance (h) is provided in Fig. 6.

When contact occurs between the virtual fibers, that is, the distance between the center line of the virtual fiber is

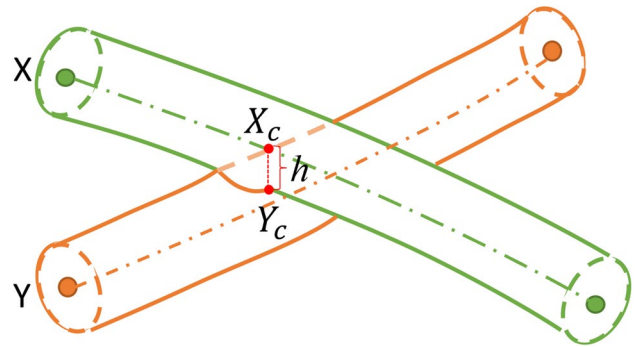


Fig. 6 Virtual fiber penetration

less than the diameter of the virtual fiber, it is necessary for us to get the minimum distance between the two. The model has three contact modes, as shown in Fig. 7. For different contacts, the shortest distances can be calculated as follows.

When the shortest distance is node-to-node contact, it can be denoted as

$$\| X_f - Y_f \| = \sqrt{\Delta x^2 + \Delta y^2 + \Delta z^2} \tag{9}$$

When the shortest distance is node-to-rode contact, it can be expressed as

$$\| X_f - Y_f \| = \frac{r_{i,i+1} \times r_{i,j}}{r_{i,i+1}} \tag{10}$$

When the shortest distance is rode-to-rode contact, $r_{i,j}$ is the vector of truss element node. It is decomposed into three

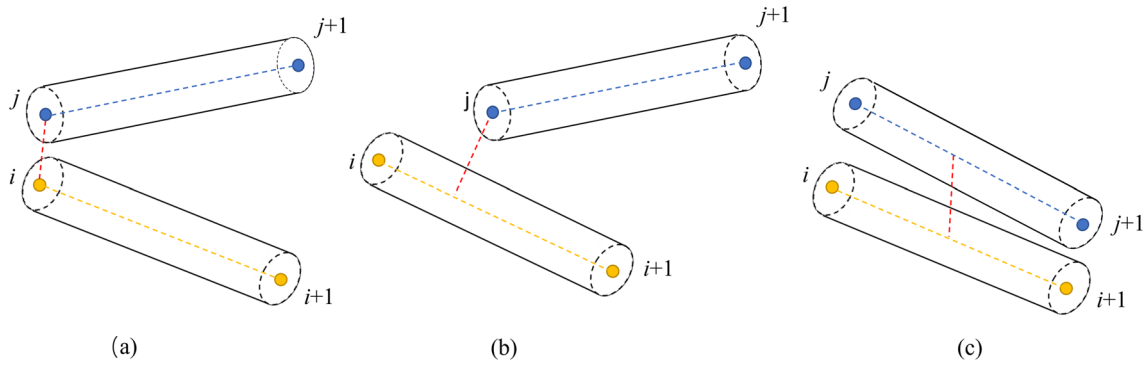


Fig. 7 Three contact methods: **a** node-to-node contact; **b** node-to-rod contact; **c** rod-to-rod contact

components. \mathbf{P} is the coordinate transformation matrix and d is the minimum distance between them. It can be expressed as

$$\mathbf{P} = [\mathbf{r}_{i,i+1} - \mathbf{r}_{j,j+1} \mathbf{r}_{i,i+1} \times \mathbf{r}_{j,j+1}] \tag{11}$$

$$\begin{pmatrix} l_1 \\ l_2 \\ d \end{pmatrix} = \mathbf{P}^{-1} \cdot \mathbf{r}_{i,j} \tag{12}$$

$$d = \| X_f - Y_f \| \tag{13}$$

The law of changes in fabric geometry

Model geometry validation

In order to verify the validity of the numerical model, the numerical model was compared with the fabric sample. In the numerical model, two planes are defined along the paths of warp and weft tows to observe the yarn shape and path inside the fabric. The numerical model was intercepted in the whole model, as shown in Fig. 8a. Figure 8b, d are the CT cross-section of the fabric sample in the warp and weft directions, respectively. Figure 8c, e show the cross-sectional view of the numerical model in the A-A plane and B-B plane. Through measurement, the thickness of the numerical model is 3.11 mm, the actual thickness of the fabric sample is 3 mm, and the error is 3.7%, which has a good consistency. The numerical model also reflected the interweaving of warp and weft, as well as the cross-section and path of warp and weft tows.

Interweaving process and weft cross-section variation characteristics

After the numerical model predicted the actual fabric structure well, the weaving process of warp and weft yarns is further studied, which is before yarn interweaving, yarn interweaving process, and after yarn interweaving, as shown in Fig. 3a-c. In fabric forming, the tension at both ends of the yarn is the main driving force. The warp yarn is gradually straightened under the action of tension, and the load force is gradually transmitted from both ends of the fabric to the middle, thus starting to interweave with the weft yarn. When interweaving, the transverse force generated by the warp tension makes the cross-sectional shape of the weft yarn gradually change from the beginning rectangle to the ellipse until it becomes more and more flat, and the cross-sectional area of the weft yarn changes. From the micro-scale view, under the influence of tension, the arrangement of fiber changes until it becomes stable. On the whole, the outer weft yarns gradually moves closer to the middle layers under the transverse force generated by the warp tension. According to the fabric weaving process, we find two characteristics of the weft cross-section. Firstly, the weft cross-section aspect ratio is getting larger, as presented in Fig. 9. As the analysis step time increases, the tension gradually increases, and the transverse force acting on the weft becomes larger. The originally neatly arranged fibers begin to move to the center and both sides under the action of external forces. From Fig. 9, we find that the cross-section of the weft yarn changes most obviously from 0 to 0.1 s, and the cross-section of the weft yarn changes lightly from 0.1 to 0.2 s. Because from 0 to 0.1 s, the load at both ends increases rapidly, raising slowly

Fig. 8 Comparison between the CT view and numerical results: **a** Intercepted numerical model; **b** CT scanning cross-section along the warp direction; **c** A-A plane cross-sectional view; **d** CT scanning cross-section along the weft direction; **e** B-B plane cross-sectional view

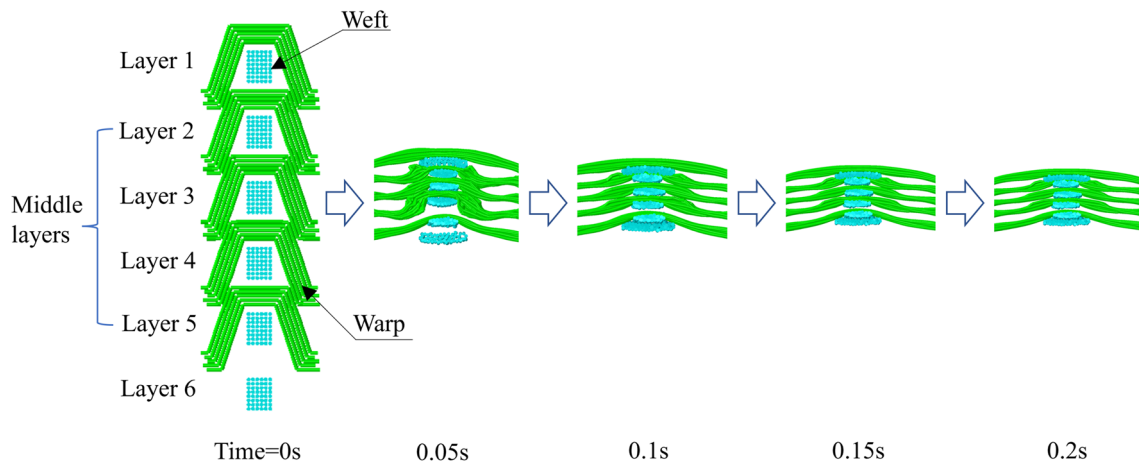
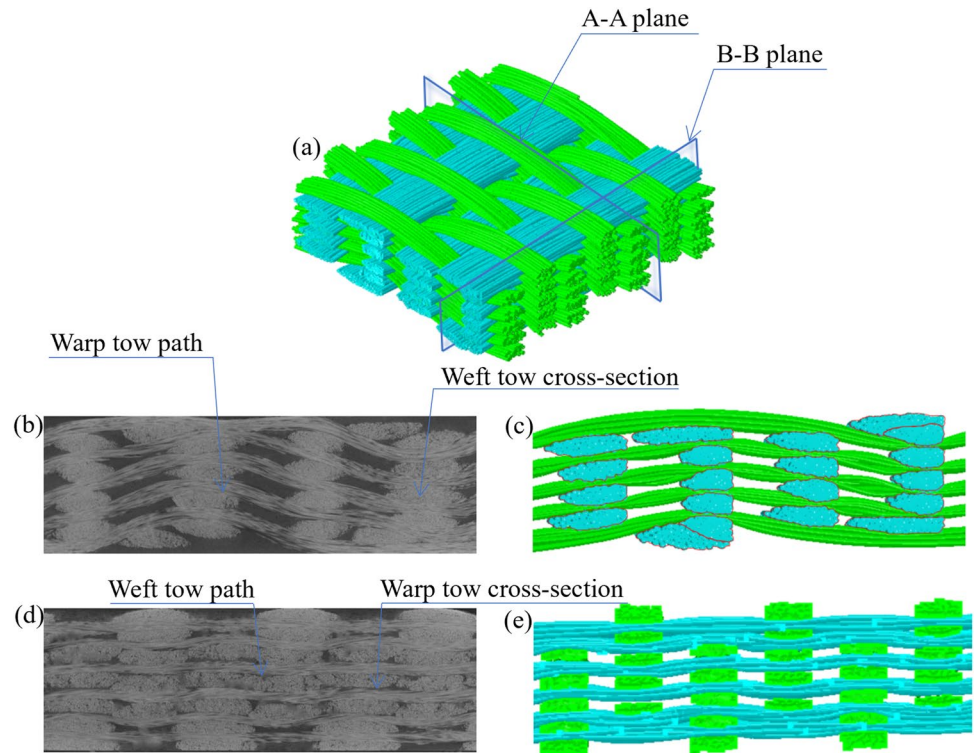


Fig. 9 Weft tows cross-section variation along the warp tow at different step times

from 0.1 to 0.2 s. The link between the step time and the load is shown in Fig. 4. Secondly, the cross-sectional area of the weft shows a downward trend. Because with the increase of the tension at both ends of the warp, the transverse force acting on the interweaving of the warp and weft will increase, and the gap between the fibers subjected to the external force will gradually decrease. In this section, a total of five-step time fabrics of 0,0.05,0.1,0.15,0.2 were selected to obtain the corresponding six-layer weft, and the cross-sectional area of each layer of weft was quantitatively measured. The

curves of the weft cross-sectional area and the analysis step time are displayed in Fig. 10a. Figure 10b presents the variation trend of each layer weft cross-section shape with the analysis step time. They reveal that the cross-sectional area of each layer of weft yarn decreases with the analysis step time. At the same analysis step time, the cross-sectional areas of the weft tows of middle layers are basically the same. The cross-sectional areas of the middle layers change more due to the extrusion of the outer layers weft tows.

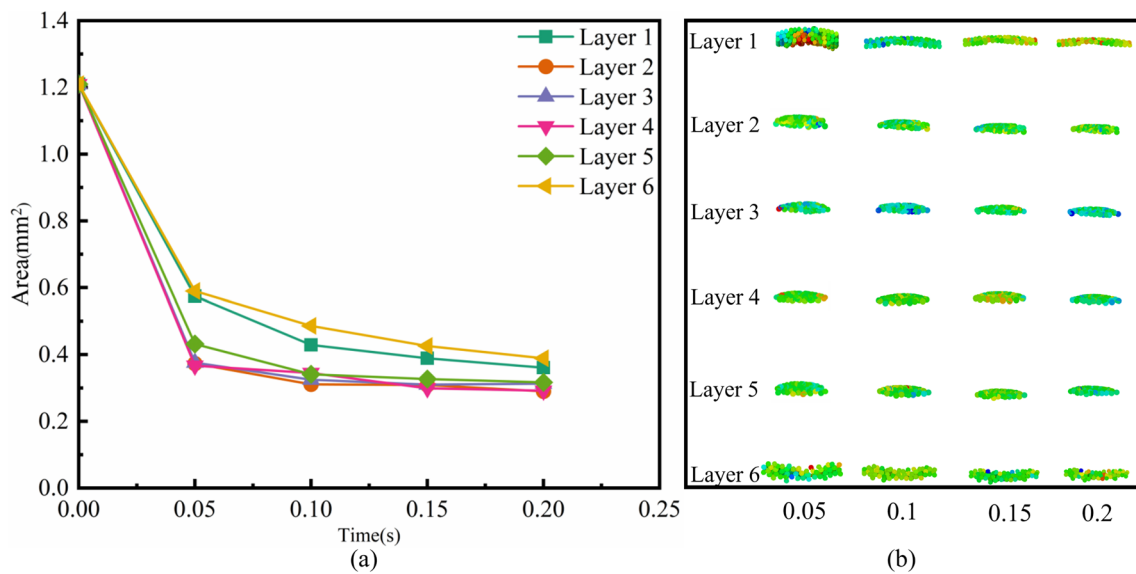


Fig. 10 a Area of the weft cross-section at different layers versus the step time; b Weft tows cross-section shapes versus the step time

Table 2 Yarn tension for each tow

Number	Warp tow (N)	Weft tow (N)
I	3	2.5
II	4	2.5
III	5	2.5

Through the above analysis, it can be concluded that the warp tows of each layer are gradually interwoven with the weft tows under the action of tension at both ends. In this process, there will be a transverse force at the interweaving with the weft tows. The transverse force applied to the weft tows will cause weft deformation. According to the analysis of the interaction force, the transmission direction of the transverse force is perpendicular to the weft tow, and the weft tension along the length of the yarn has little effect on the change of the cross-section of the yarn. In summary, the micro-structure of the fabric is affected by the fiber rearrangement so that the fabric is deformed macroscopically. The transverse force generated by the warp tension is the root cause of the change in the cross-sectional shape of the weft tow.

Effect of warp tension on weft tow geometry

According to the above analysis, it is concluded that the transverse force generated by the warp tension is the main factor for the change of the weft cross-section shape. In the previous section, the tension at both ends of the warp was set to 3 N, and two additional groups of loads were added.

Therefore, three kinds of warp tension were set, and the weft tension remained unchanged. The relevant parameters are listed in Table 2.

The cross-section shape and path of the weft tow is directly affected by the warp tension at its interweaving place. In this section, the cross-section of the warp and weft interweaving under three tensions is intercepted, and the position is provided in Fig. 11a. Obvious weft tow crimps are found as shown in Fig. 12b. Figure 11b presents the cross-sectional areas of the weft tows under different tension configurations by measuring middle six-layer weft tows. Figure 11c displays each weft tow cross-sectional shapes. Although the cross-sectional shape of the weft yarn will not change significantly as the tension increases, the cross-sectional area will become smaller, the area of 3 to 4 N changes greatly, and the area of 4 to 5 N changes little. With the tension at both ends of the warp from 3 to 5 N, the thickness of the fabric decreases, which significantly improves the tightness of the fabric. Figure 12a shows the weft tow crimp angle under different tension configurations. By measuring the position where the crimp occurs at the interweaving of the warp and weft tows, as the warp tension changes from 3 to 5 N, the crimp angle will also increase, but the amplitude will decrease.

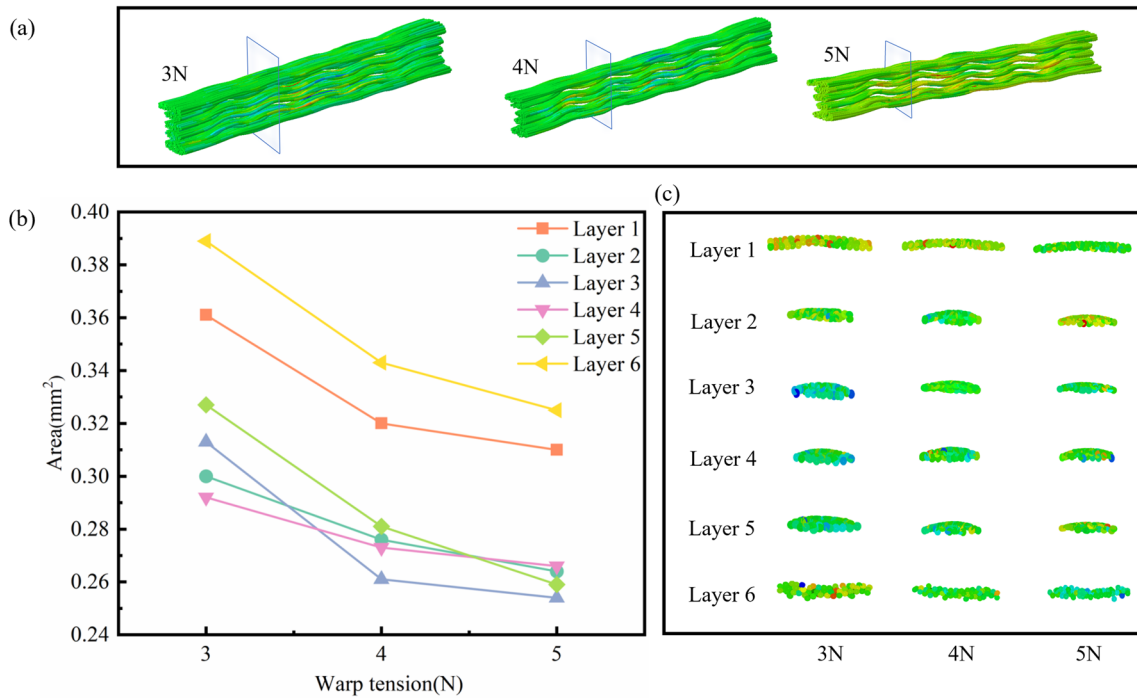


Fig. 11 a Weft cross-section position for three types of tension; b Area of each layer of weft cross-section under three tension configurations; c Weft tows cross-section shapes under three kinds of tension

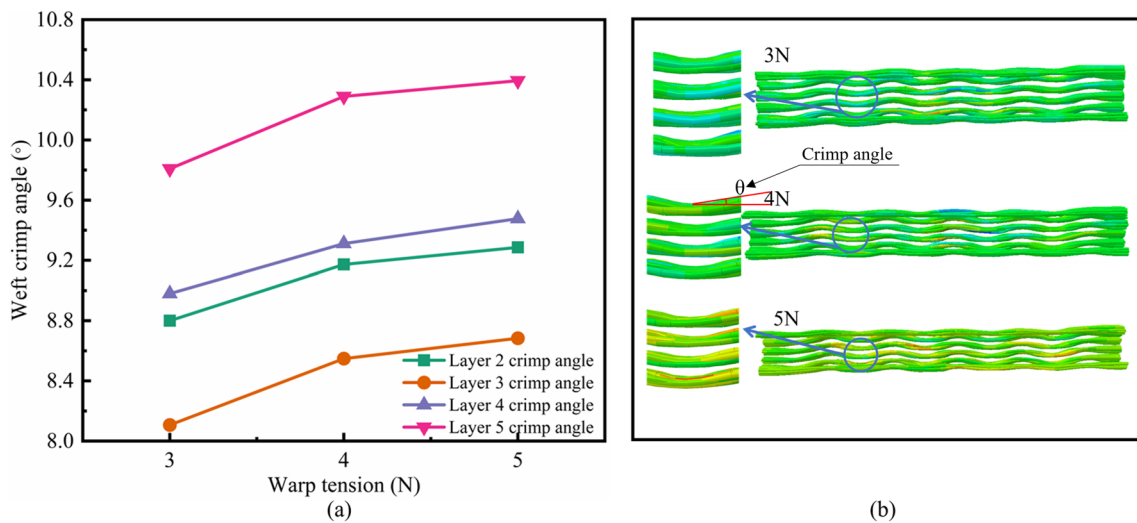


Fig. 12 a Comparison of weft crimp angles for three tension configurations; b Weft crimp position for three tension configurations

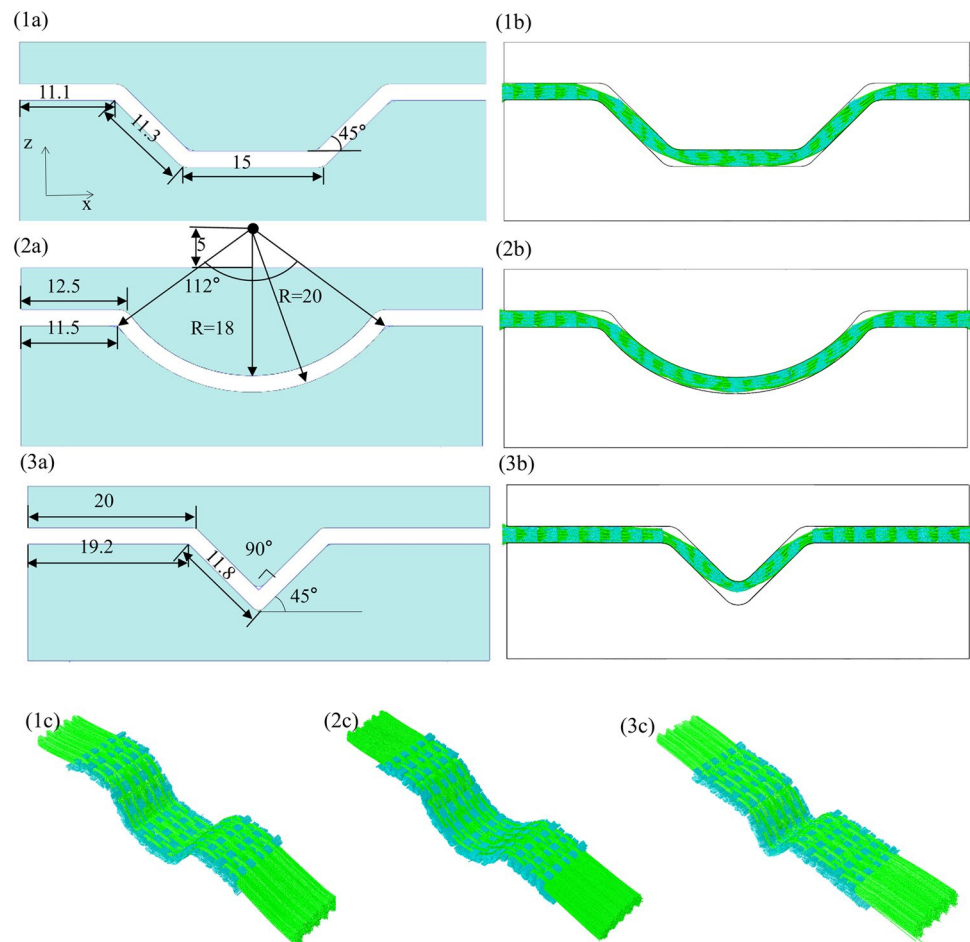
Fabric compression mechanism studies

Simulation design of finite element compressed fabric

In this section, a numerical model of compressed fabric was established based on fabric stretch forming to predict

the change in the internal structure of fabric under external compression. A total of three shapes of molds were designed, which were semi-hexagonal, circular arc, and L-shaped. The fabric compression modeling and simulation process can conclude in the three steps. (1) According to the size of the stretched fabric, the corresponding mold size was designed and modeled in the modeling software UG. Figure 131a-3a present the specific size of the three

Fig. 13 **1a-3a** Three types of mold size view; **1b-3b** The state of fabric compression completion; **1c-3c** Axonometric view of fabric compression completion

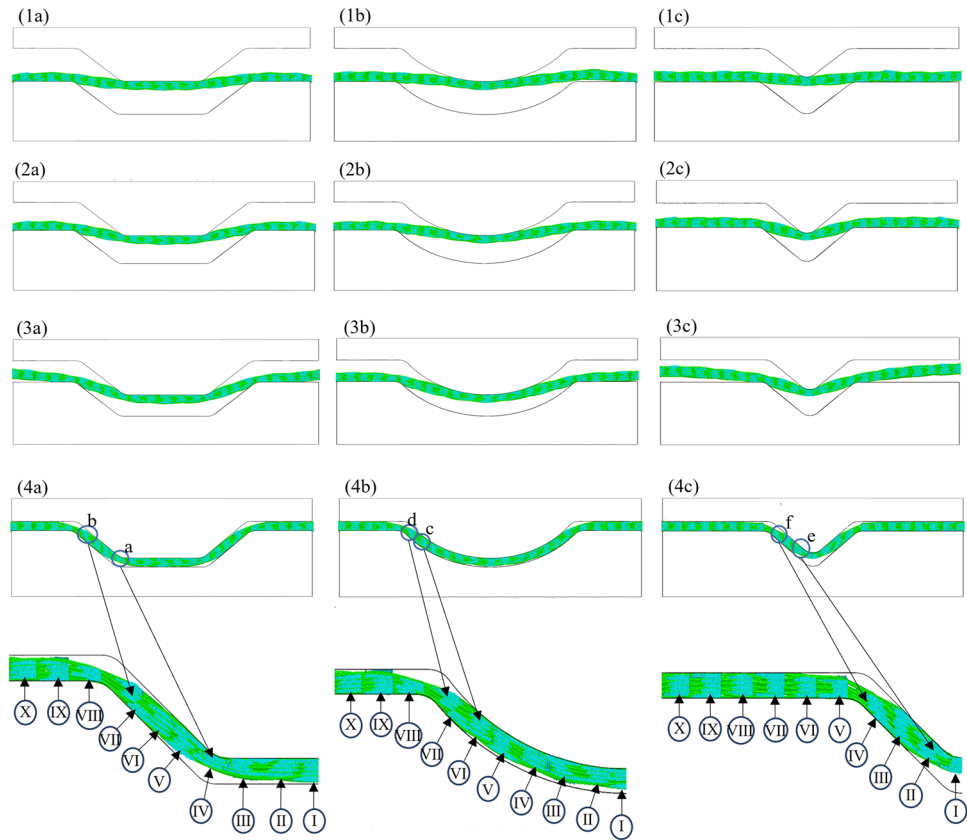


molds. In order to determine the coordinates of the outer contour points of the mold, a point was selected as the reference origin. (2) To reduce the simulation time, the solid model was changed into a discrete rigid body, and the shape of the shell was selected when using the finite element simulation software Abaqus for modeling. The fabric stretching process was the first analysis step (Step1), and the second analysis step (Step2) was added as the compression process. The compression process time, the contact between the fibers inside the yarn tow, and the contact between the upper mold and the lower mold were set in Abaqus. In the compression process, the lower mold had 0 degrees of freedom, and the upper mold had only one degree of freedom of translation in the thickness-direction. (3) By using the dynamic explicit solver in Abaqus to solve the fabric compression process. This solver is well suited to handle the complex contact between fibers and the highly nonlinear deformation. The compression results of the three shapes are presented in Fig. 131b-3b, and the fabric axonometric diagrams after compression are shown in Fig. 131c-3c.

The compression process of the fabric

In the compression process, the mold compressed the fabric to a uniform thickness of 2 mm, and the compression was completed. Considering the symmetry of the mold, this section analyzed the left region. The figures a, b and c represent three shape compression processes, respectively. From the beginning of compression to compression process until the end of compression, a total of four compression states of the same analysis step time were selected. The overall deformation of the fabric during compression of the semi-hexagonal mold is shown in Fig. 141a-4a. The lower mold was fixed, and the upper mold moved downward along the z-axis. The lower corner of the upper mold and the upper corner of the lower mold first started to contact the fabric, squeezing the nearby weft columns to make them slip between layers. At the end of the fabric forming, there were gaps at the upper and lower corner of the mold. The Fig. 141b-4b show the process of compressing the fabric with the circular arc mold. The center arc part of the upper mold and the corner of the lower mold first began to squeeze the fabric, and the arc

Fig. 14 **1a-4a** Process of semi-hexagonal compression fabric; **1b-4b** Process of circular arc compression fabric; **1c-4c** Process of L-shaped compression fabric



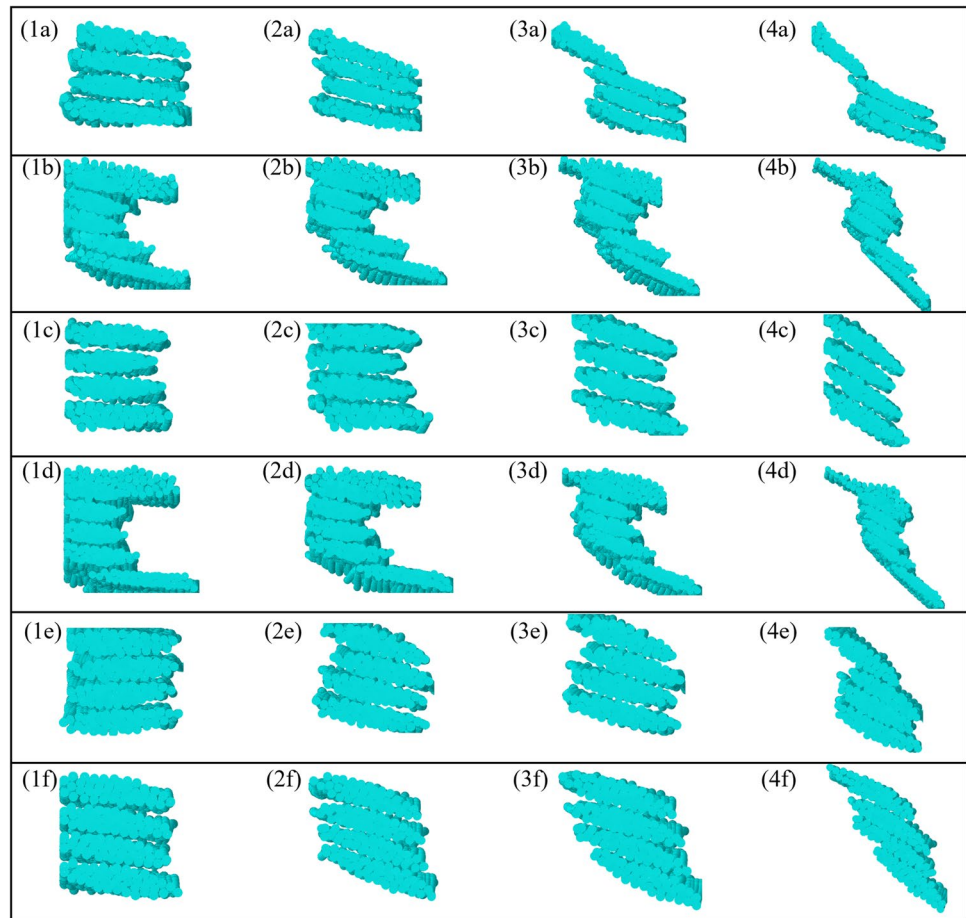
region of the fabric bulged, and the adjacent weft columns slipped between layers. In the end, the upper corner of the mold had a gap. The process of compressing the fabric with L-shaped mold is shown in Fig. 141c-4c. The convex part of the upper mold and the corner of the lower mold were the first to contact the fabric, and the surrounding weft columns also slipped between layers under extrusion. When the compression was completed, there were gaps at the upper and lower corners of the mold. The three shapes of the molds compressed the fabric, and the fabric started from the beginning of the stretch until the final bending state, and the inter-layer slip became more and more obvious.

From Fig. 14, it can be found that the weft columns slip occurred most obviously at the corner of the mold, which were marked with blue circles. The deformation of the weft column at the corresponding corner is shown in Fig. 15. When the fabric was compressed by a semi-hexagonal mold, the weft column changes at the corners corresponding to the four states of the compression process are shown in Fig. 151a-4a, 1b-4b. The four-layer weft columns (at the lower corner) were arranged neatly at the beginning of compression as shown in Fig. 151a. As shown in Fig. 152a, the whole weft column had a small slip. Figure 153a, 4a show that as the lower corner of the upper mold further pressed down until the end of compression, the uppermost weft tow of the four-layer weft column had a large slip along

the upper- left direction. The six-layer weft column (at the upper corner) maintained the C-shaped trend during stretching at the beginning of compression, and then the bottom two layers of weft tows had a certain slip along the lower-right direction, as shown in Fig. 151b, 2b. Figure 153b, 4b display that with the pressing of the upper mold, the upper corner of the lower mold squeezed, and the six-layer weft column slipped greatly. When the fabric was compressed by the circular arc mold, the weft column variations at the corners corresponding to the four states of the compression process are shown in Fig. 151c-4c, 1d-4d. Figure 151c-4c show that the four-layer weft column (at the upper corner) was arranged from neat to slip during the gradual pressing of the upper mold. The changes of the six-layer weft column (at the upper corner) were basically the same as the fabric was compressed in a half-hexagonal mold. When the L-shaped compressed, the changes of the weft column at the corner corresponding to the four states of the compression process is shown in Fig. 151e-4e, 1f-4f. The four-layer weft columns located at the lower and upper corners of the mold, respectively, changed from neat to slip. The weft column at the upper corner had a larger slip.

By observing the compression results of three different shapes, it can be found that the gap between the fabric and the mold occurred at the corner. This is due to the large deformation of the fabric at the corner, where the weft

Fig. 15 **1a-4a** and **(1b-4b)** The changes of weft columns at the corner of semi-hexagonal mold; **1c-4c** and **(1d-4d)** The changes of weft columns at the corner of circular arc mold; **1e-4e** and **(1f-4f)** The changes of weft columns at the corner of L-shaped mold



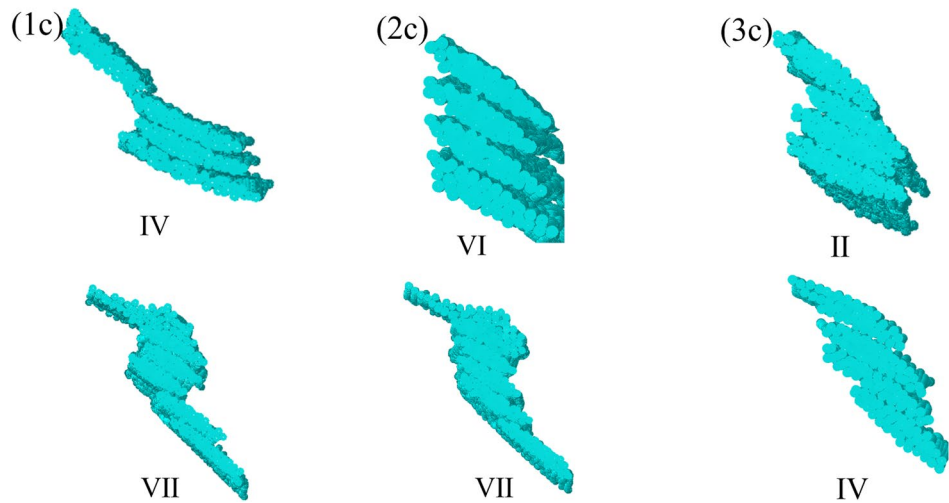
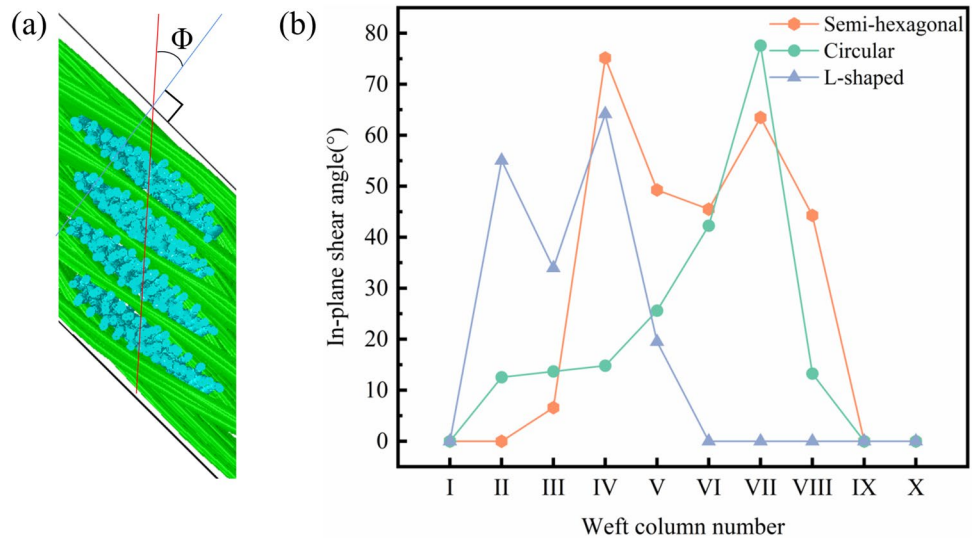
column is squeezed and slipped to both sides. In order to reduce the gap between the fabric and the corner of the mold, the thickness of the fabric can be appropriately increased.

Simulation results and analysis

By observing the numerical simulation results of the compressed fabric, it can be found that the inter-layer slip occurred inside the fabric. Based on the analysis of the mold compression process in the previous section, it was found that the inter-layer slip is more obvious in the region (at the corner) with large deformation of the mold. In order to quantitatively describe this deformation, the inter-layer shear angle Φ is introduced to quantify the inter-layer deformation of the 3D preform in compression molding. The definition of Φ is displayed in Fig. 16a. Line-1 (the red solid line) is determined by connecting the centroids of yarn cross-sections located at the surface and bottom layers. Line-2 (the blue solid line) is the normal line of the point on the surface. When the line-1 is perpendicular to the surface of the preform, there is no inter-layer deformation. Considering the symmetry of the three types of molds, only 1/2 region was measured on the left side of

the surface for each compression simulation result. The inter-layer shear angles were measured from the center of the mold to the left, a total of 10 groups, using Roman numerals (I-X) to represent the weft columns as shown in Fig. 14. The measurement results are presented in Fig. 16b. Judging from the measurement results, it reveals that when the semi-hexagonal mold compresses fabric, the most severe inter-layer slip occurred in weft columns IV and VII, in Fig. 161c, which occurred at the upper and lower corners on the left side of the mold. The most significant inter-layer slip occurred in weft columns VI and VII when the circular arc mold compressed fabric, as shown in Fig. 162c. At the transition region of the circular and planar, the inter-layer shear angle reached the peak. At the region near the center of the circular, the inter-layer shear angle was small. For the L-shaped mold, the most significant inter-layer slip occurred in the weft columns II and IV, as displayed in Fig. 163c, which occurred near the right angle and the upper corner. In conclusion, the results of quantitative measurement were consistent with the analysis of mold compression process, which further verified the correction of the analysis in the previous section.

Fig. 16 **a** Definition of the inter-layer shear angle Φ ; **b** The in-plane shear angle of each weft column; **1c-3c** The weft column with the most obvious inter-layer slip in each type of simulation



Conclusions

A simulation method based on virtual fiber was proposed to predict the micro-geometric structure of 3D angle-interlock woven fabric. The yarn behavior can be well represented by using truss element chains to simulate the virtual fibers. The main conclusions can be drawn according to obtained results.

- (1) The finite element analysis software Abaqus was used to run the written Python script to generate the initial loose fabric model. An accurate 3D angle-interlock woven fabric model was obtained by applying loads at both ends of the yarn. The micro-geometric structure of the model was in good agreement with the CT scan results of the actual fabric samples.
- (2) By measuring the cross-sectional area of each layer of weft tow in the center of the numerical model at different analysis steps, it was found that the cross-sectional

area of each layer of weft tow had a decreasing trend. The analysis showed that the cross-sectional geometry of the weft tow was mainly affected by the transverse force generated by the warp tension at the interweave with the weft tow. This paper further investigated the different tensions (3 N, 4 N, 5 N) on the specified cross-section (warp and weft interweaving place), and got the result that the weft cross-sectional area was reduced. Meanwhile, the warp tension will affect the path of the weft tow. At the interweaving region, Weft tow will generate crimp angle. This paper also explored the influence of different tension(3 N,4 N,5 N) on the crimp angle, and obtained the result that the rise of warp tension will lead to the increase of crimp angle.

- (3) Three kinds of special-shaped molds were created to simulate fabric compression. It was revealed that inter-layer slip occurred inside the fabric. The inter-layer shear angle was introduced to describe this deformation quantitatively. The result indicated that the most

significant inter-layer slip occurred at the corner of the mold (the part with large deformation), and the slip trend was related to the shape of the mold.

- (4) The simulation method proposed in this paper applies not only to 3D angle-interlock woven fabrics but also to other general 3D fabrics. It provides a feasible method for 3D fabric micro-geometry prediction. Numerical simulation of compression is of great significance for predicting preforms with complex shapes.

Acknowledgements The authors gratefully acknowledge the great support from the National Natural Science Foundation of China (Grant No. 52075498, 11702249, U22A20182).

Declarations

Competing interests The authors declare that they have no known competing financial interests or personal relationships that could have appeared to influence the work reported in this paper.

References

- Mouritz AP, Cox BN (2010) A mechanistic interpretation of the comparative in-plane mechanical properties of 3D woven, stitched and pinned composites. *Compos Appl Sci Manuf* 41(6):709–728. <https://doi.org/10.1016/j.compositesa.2010.02.001>
- Chen X, Taylor LW, Tsai LJ (2011) An overview on fabrication of three-dimensional woven textile preforms for composites. *Text Res J* 81(9):932–944. <https://doi.org/10.1177/0040517510392471>
- Bilisik K (2012) Multiaxis three-dimensional weaving for composites: a review. *Text Res J* 82(7):725–743. <https://doi.org/10.1177/0040517511435013>
- Potluri P, Manan A, Young R, Lei S (2007) Experimental validation of micro-strains predicted by Meso-scale Models for Textile Composites. In: 48th AIAA/ASME/ASCE/AHS/ASC Structures, Structural Dynamics, and Materials Conference. <https://doi.org/10.2514/6.2007-2159>
- Schuster J, Heider D, Sharp K, Glowania M (2008) Thermal conductivities of three-dimensionally woven fabric composites. *Compos Sci Technol* 68(9):2085–2091. <https://doi.org/10.1016/j.compscitech.2008.03.024>
- Shan Z, Chen S, Zhang Q, Qiao J, Wu X, Zhan L (2016) Three-dimensional woven forming technology and equipment. *J Compos Mater* 50(12):1587–1594. <https://doi.org/10.1177/002198315590267>
- Renaud J, Vernet N, Ruiz E, Lebel LL (2016) Creep compaction behavior of 3D carbon interlock fabrics with lubrication and temperature. *Compos Appl Sci Manuf* 86:87–96. <https://doi.org/10.1016/j.compositesa.2016.04.017>
- Behera BK, Dash BP (2015) Mechanical behavior of 3D woven composites. *Mater Des* 67:261–271. <https://doi.org/10.1016/j.matdes.2014.11.020>
- Yan S, Zeng X, Long A (2019) Meso-scale modelling of 3D woven composite T-joints with weave variations. *Compos Sci Technol* 171:171–179. <https://doi.org/10.1016/j.compscitech.2018.12.024>
- Gereke T, Döbrich O, Hübner M, Cherif C (2013) Experimental and computational composite textile reinforcement forming: a review. *Compos Appl Sci Manuf* 46:1–10. <https://doi.org/10.1016/j.compositesa.2012.10.004>
- Naouar N, Vasiukov D, Park CH, Lomov SV, Boisse P (2020) Meso-FE modelling of text-ile composites and X-ray tomography. *J Mater Sci* 55:16969–16989. <https://doi.org/10.1016/j.compscitech.2015.11.023>
- Vanaerschot A, Cox BN, Lomov SV, Vandepitte D (2016) Experimentally validated stochastic geometry description for textile composite reinforcements. *Compos Sci Technol* 122:122–129. <https://doi.org/10.1016/j.compscitech.2015.11.023>
- El Said B, Ivanov D, Long AC, Hallet SR (2016) Multi-scale modelling of strongly heterogeneous 3D composite structures using spatial Voronoi tessellation. *J Mech Phys Solids* 88:50–71. <https://doi.org/10.1016/j.jmps.2015.12.024>
- Miao Y, Zhou E, Wang Y, Cheeseman BA (2008) Mechanics of textile composites: micro-geometry. *Compos Sci Technol* 68(7–8):1671–1678. <https://doi.org/10.1016/j.compscitech.2008.02.018>
- Nilakantan G (2013) Filament-level modeling of Kevlar KM2 yarns for ballistic impact studies. *Compos Struct* 104:1–13. <https://doi.org/10.1016/j.compstruct.2013.04.001>
- Samadi R, Robitaille F (2014) Particle-based modeling of the compaction of fiber yarns and woven textiles. *Text Res J* 84(11):1159–1173. <https://doi.org/10.1177/0040517512470200>
- Sockalingam S, Gillespie JW Jr, Keefe M (2017) Modeling the fiber length-scale response of Kevlar KM2 yarn during transverse impact. *Text Res J* 87(18):2242–2254. <https://doi.org/10.1177/0040517516669074>
- Grujicic M, Hariharan A, Pandurangan B, Yen CF, Cheeseman BA, Wang Y, Zheng JQ (2012) Fiber-level modeling of dynamic strength of Kevlar® KM2 ballistic fabric. *J Mater Eng Perform* 21:1107–1119
- Wang Y, Sun X (2001) Digital-element simulation of textile processes. *Compos Sci Technol* 61(2):311–319. [https://doi.org/10.1016/S0266-3538\(00\)00223-2](https://doi.org/10.1016/S0266-3538(00)00223-2)
- Zhou G, Sun X, Wang Y (2004) Multi-chain digital element analysis in textile mechanics. *Compos Sci Technol* 64(2):239–244. [https://doi.org/10.1016/S0266-3538\(03\)00258-6](https://doi.org/10.1016/S0266-3538(03)00258-6)
- Döbrich O, Gereke T, Cherif C (2014) Modelling of textile composite reinforcements on the micro-scale. *Autex Res J* 14(1):28–33. <https://doi.org/10.2478/v10304-012-0047-z>
- Döbrich O, Gereke T, Cherif C (2016) Modeling the mechanical properties of textile-reinforced composites with a near micro-scale approach. *Compos Struct* 135:1–7. <https://doi.org/10.1016/j.compstruct.2015.09.010>
- Mahadik Y, Hallett SR (2010) Finite element modelling of tow geometry in 3D woven Fabrics. *Compos Appl Sci Manuf* 41(9):1192–1200. <https://doi.org/10.1016/j.compositesa.2010.05.001>
- Green SD, Long AC, El Said BSF, Hallett SR (2014) Numerical modelling of 3D woven preform deformations. *Compos Struct* 108:747–756. <https://doi.org/10.1016/j.compstruct.2013.10.015>
- Daelemans L, Faes J, Allaoui S, Hivet G, Dierick M, Van Hoorbeke L, Van Paepegem W (2016) Finite element simulation of the woven geometry and mechanical behaviour of a 3D woven dry fabric under tensile and shear loading using the digital element method. *Compos Sci Technol* 137:177–187. <https://doi.org/10.1016/j.compscitech.2016.11.003>
- Sockalingam S, Gillespie JW Jr, Keefe M (2014) On the transverse compression response of Kevlar KM2 using fiber-level finite element model. *Int J Solids Struct* 51(13):2504–2517. <https://doi.org/10.1016/j.ijsolstr.2014.03.020>
- Sockalingam S, Gillespie JW Jr, Keefe M (2017) Role of inelastic transverse compressive behavior and multiaxial loading on the transverse impact of Kevlar KM2 single fiber. *Fibers* 5(1):9. <https://doi.org/10.3390/fib5010009>
- Sockalingam S, Gillespie JW Jr, Keefe M (2015) Dynamic modeling of Kevlar KM2 single fiber subjected to transverse impact.

- Int J Solids Struct 67:297–310. <https://doi.org/10.1016/j.ijsolstr.2015.04.031>
29. De Luycker E, Morestin F, Boisse P, Marsal D (2009) Simulation of 3D interlock composite preforming. *Compos Struct* 88(4):615–623. <https://doi.org/10.1016/j.compstruct.2008.06.005>
 30. Xiao S, Wang P, Soulat D, Gao H (2020) An exploration of the deformability behaviours dominated by braiding angle during the forming of the triaxial carbon fibre braids. *Compos Appl Sci Manuf* 133:105890. <https://doi.org/10.1016/j.compositesa.2020.105890>
 31. Jiao W, Chen L, Xie J, Yang Z (2022) Deformation mechanisms of 3D LTL woven preforms in hemisphere forming tests. *Compos Struct* 283:115156. <https://doi.org/10.1016/j.compstruct.2021.115156>
 32. Abteu MA, Boussu F, Bruniaux P, Loghin C, Cristian I, Chen Y, Wang L (2018) Influences of fabric density on mechanical and moulding behaviours of 3D warp interlock para-aramid fabrics for soft body armour application. *Compos Struct* 204:402–418. <https://doi.org/10.1016/j.compstruct.2018.07.101>
 33. Durville D (2010) Simulation of the mechanical behaviour of woven fabrics at the scale of fibers. *Int J Mater Form* 3:1241–1251. <https://doi.org/10.1007/s12289-009-0674-7>

Publisher's Note Springer Nature remains neutral with regard to jurisdictional claims in published maps and institutional affiliations.

Springer Nature or its licensor (e.g. a society or other partner) holds exclusive rights to this article under a publishing agreement with the author(s) or other rightsholder(s); author self-archiving of the accepted manuscript version of this article is solely governed by the terms of such publishing agreement and applicable law.